NRC·CNRC

NRC Publications Archive
Archives des publications du CNRC

Learnable weight graph neural network for river ice classification

Qu, Yifan; Soleymani, Armina; Sudom, Denise; Scott, K. Andrea

This publication could be one of several versions: author's original, accepted manuscript or the publisher's version. / La version de cette publication peut être l'une des suivantes : la version prépublication de l'auteur, la version acceptée du manuscrit ou la version de l'éditeur.

For the publisher's version, please access the DOI link below./ Pour consulter la version de l'éditeur, utilisez le lien DOI ci-dessous.

Publisher's version / Version de l'éditeur:

https://doi.org/10.3390/proceedings2024110030

MDPI Proceedings, 110, 1, 2025-01-13

NRC Publications Archive Record / Notice des Archives des publications du CNRC :

https://nrc-publications.canada.ca/eng/view/object/?id=7932424b-75e6-45c2-86a6-f16ebacf0b98

https://publications-cnrc.canada.ca/fra/voir/objet/?id=7932424b-75e6-45c2-86a6-f16ebacf0b98

Access and use of this website and the material on it are subject to the Terms and Conditions set forth at

https://nrc-publications.canada.ca/eng/copyright

READ THESE TERMS AND CONDITIONS CAREFULLY BEFORE USING THIS WEBSITE.

L'accès à ce site Web et l'utilisation de son contenu sont assujettis aux conditions présentées dans le site

https://publications-cnrc.canada.ca/fra/droits

LISEZ CES CONDITIONS ATTENTIVEMENT AVANT D'UTILISER CE SITE WEB.

Questions? Contact the NRC Publications Archive team at PublicationsArchive-ArchivesPublications@nrc-cnrc.gc.ca. If you wish to email the authors directly, please see the first page of the publication for their contact information.

Vous avez des questions? Nous pouvons vous aider. Pour communiquer directement avec un auteur, consultez la première page de la revue dans laquelle son article a été publié afin de trouver ses coordonnées. Si vous n'arrivez pas à les repérer, communiquez avec nous à PublicationsArchive-ArchivesPublications@nrc-cnrc.gc.ca.

National Research Council Canada | Conseil national de recherches Canada

Canada

proceedings

MDPI

Proceeding Paper

Learnable Weight Graph Neural Network for River Ice Classification †

Yifan Qu [1], Armina Soleymani [2], Denise Sudom [3] and Katharine Andrea Scott [2,*]

[1] Department of Applied Math, University of Waterloo, Waterloo, ON N2L 3G1, Canada; quyf0516@outlook.com
[2] Department of Mechanical and Mechatronics Engineering, University of Waterloo, Waterloo, ON N2L 3G1, Canada; armina.soleymani@uwaterloo.ca
[3] National Research Council Canada, Ottawa, ON K1A 0R6, Canada; denise.sudom@nrc-cnrc.gc.ca
* Correspondence: ka3scott@uwaterloo.ca
† Presented at the 31st International Conference on Geoinformatics, Toronto, ON, Canada, 14–16 August 2024.

Abstract: Monitoring river ice is crucial for planning safe navigation routes, with ice–water classification being one of the most important tasks in ice mapping. While high-resolutions satellite imagery, such as synthetic aperture radar (SAR), is well-suited to this task, manual interpretation of these data is challenging due to the large data volume. Machine learning approaches are suitable methods to overcome this; however, training the models might not be time-effective when the desired result is a narrow structure, such as a river, within a large image. To address this issue, we proposed a model incorporating a graph neural network (GNN), called learnable weights graph convolution network (LWGCN). Focusing on the winters of 2017–2021 with emphasis on the Beauharnois Canal and Lake St Lawrence regions of the Saint Lawrence River. The model first converts the SAR image into graph-structured data using simple linear iterative clustering (SLIC) to segment the SAR image, then connecting the centers of each superpixel to form graph-structured data. For the training model, the LWGCN learns the weights on each edge to determine the relationship between ice and water. By using the graph-structured data as input, the proposed model training time is eight times faster, compared to a convolution neural network (CNN) model. Our findings also indicate that the LWGCN model can significantly enhance the accuracy of ice and water classification in SAR imagery.

Keywords: graph neural network; river ice; classification; synthetic aperture radar

check for updates

Citation: Qu, Y.; Soleymani, A.; Sudom, D.; Scott, K.A. Learnable Weight Graph Neural Network for River Ice Classification. *Proceedings* **2024**, *110*, 30. https://doi.org/10.3390/proceedings2024110030

Academic Editors: Dongmei Chen, Yuhong He and Songnian Li

Published: 13 January 2025

Copyright: © 2025 by the authors. Licensee MDPI, Basel, Switzerland. This article is an open access article distributed under the terms and conditions of the Creative Commons Attribution (CC BY) license (https://creativecommons.org/licenses/by/4.0/).

1. Introduction

Classifying ice from water in river ice imagery is challenging due to the sparse river structure and the influence of various factors on ice formation and development, such as air temperature, river flow characteristics, and water temperature [1]. Ice mapping using remote sensing images, particularly synthetic aperture radar (SAR), is a widely used technique [2]. SAR sensors, which utilize active remote sensing, provide advantages such as high spatial resolution (unlike passive microwave data) and the capability to penetrate cloud cover (unlike optical and thermal infrared data). However, generating ice maps with extensive spatial coverage and high temporal resolution necessitates a fully or partially automated analysis of SAR imagery.

Ice and water classification is one of the most important tasks when it comes to ice mapping. Recent studies have underscored the effectiveness of machine learning methods such as convolutional neural networks (CNNs) in river ice and water classification (e.g., [3–6]). The lack of sufficient ground-truth pixel-based samples limits the training of fully supervised CNN-based methods, making their reliability uncertain across different times and locations. Moving from pixel-level to polygon-based (or region-based) classification offers more robust and easily acquired labels [7]. To address limited training data, semi-supervised graph-based neural networks (GNNs) have been used for image classification in previous

studies (e.g., [8,9]). The GNNs, particularly graph convolutional networks (GCNs) [10], effectively capture the intrinsic geometry of complex spatial domains (such as rivers) and can offer reduced computational costs compared to pixel-based methods.

In this study, we proposed a graph-based classification method to identify superpixels in SAR imagery as either ice or water, aiming to establish an efficient, timely, and cost-effective pipeline for river ice monitoring. Our model, named learnable weight graph neural network (LWGNN), employs simple linear iterative clustering (SLIC) [11] to segment SAR images into superpixels. The centers of these superpixels are then connected to form nodes in a GNN, with edges representing the connections between neighboring superpixel centers. Before training, land areas are removed from the graph to enhance the model performance. The performance of the proposed model is then compared with a CNN, a super vector machine (SVM), and the original GNN.

2. Materials and Methods

2.1. Study Region

The Beauharnois Canal and Lake Saint Lawrence sections of the Saint Lawrence were selected for sea ice classification from January to March over five consecutive years of 2017–2021 (Figure 1). These sections are part of a major corridor supporting significant vessel traffic and various infrastructure assets. The Beauharnois Canal, upstream of Montreal, is a key shipping route bypassing rapids and connecting Lake Saint Francis to Lake Saint Louis. Lake Saint Lawrence, a reservoir upstream of the Moses–Saunders power dam, plays an essential role in controlling water flow and managing ice conditions during winter to prevent issues like ice jams and build-up of frazil ice, which can clog water intakes and cause flooding [12]. Ice and water classification in these sections can be helpful for ensuring the safe and efficient management of the waterway and mitigating the future risks associated with climate change.

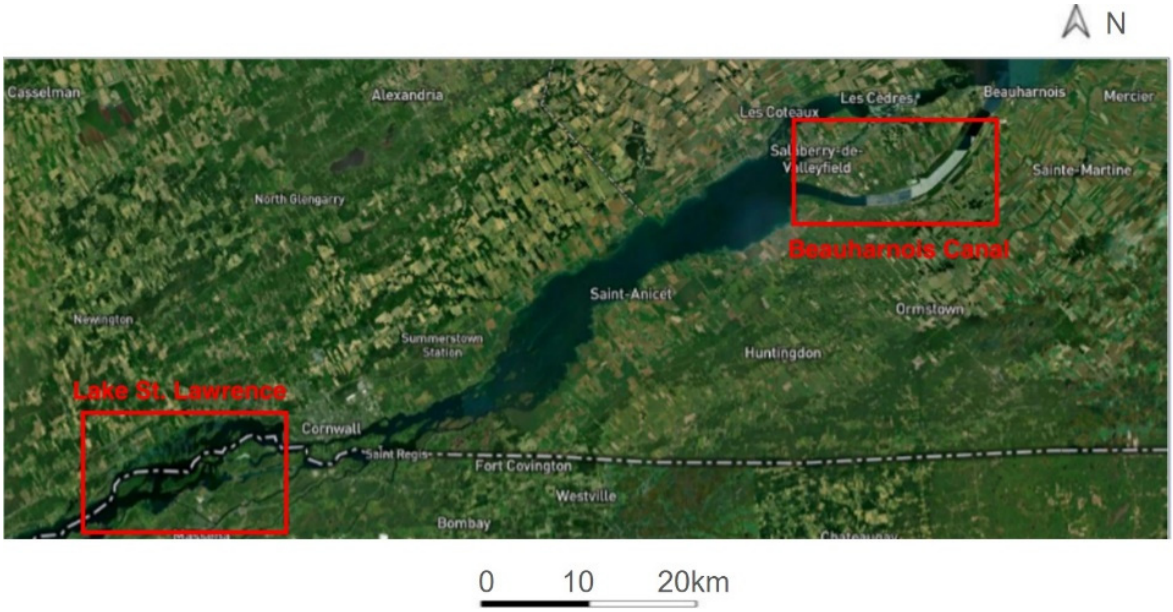

Figure 1. The study region consists of the Beauharnois Canal and Lake Saint Lawrence. The central coordinates for the Beauharnois Canal are approximately 45.26° N and 73.94° W. The central coordinates for Lake Saint Lawrence are approximately 44.99° N and 74.88° W.

2.2. Dataset

2.2.1. Sentinel-1 SAR Data

The SAR data used in this study, with a 10 m pixel spacing, correspond to the VV (vertical transmit, vertical receive) polarization channel from Sentinel-1 (C-band,

5.410 GHz). These Level-1-detected, high-resolution dual-polarization (GRD-HD) images were acquired from the Alaska Satellite Facility [13] in the interferometric wide mode. The total number of available scenes was 70 for the Beauharnois Canal and 35 scenes for Saint Lawrence Lake.

2.2.2. MODIS Data

To complement the SAR analysis, we checked the optical imagery from the moderate resolution imaging spectroradiometer (MODIS) satellite using NASA Worldview [14]. This step was done to facilitate accurate differentiation between ice and water for dates when clear-sky imagery was available, to aid the manual labeling process.

2.2.3. Land Coverage Data

To accurately exclude land from the SAR analysis, we obtained land coverage data from ESRI Land Cover Explorer [15]. This repository provides a series of land cover datasets derived from ESA Sentinel-2 satellite imagery at 10 m resolution.

2.2.4. Air Temperature Data

Given the correlation between air temperature and ice formation, we incorporated this variable into the proposed model. The air temperature data, in Celsius, was obtained from Moose Creek Wells station (the central coordinates for this station are approximately 45.26° N and 74.97° W), the nearest weather station to Lake Saint Lawrence. The data was downloaded from the Government of Canada, Environment and Natural Resources website [16]. The air temperature values were obtained at the same time as the SAR acquisition on the specified date.

2.2.5. Data Preprocessing

Thermal noise correction and calibration (for σ_0) for the Sentinel-1 SAR scenes in the dataset were carried out using the NERSC algorithm [17]. The scenes were then precisely cropped to focus on the Beauharnois Canal and Lake Saint Lawrence.

2.2.6. Class Imbalance Issue

Our analysis showed that the ice occupies mostly below 50% of the Beauharnois Canal and Lake Saint Lawrence during different times of the study period. This class imbalance issue was a challenge since the model tended to disproportionately classify the regions as water. To address this issue, we applied class weights to the loss function. These weights were calculated as the inverse frequency of each class to ensure their sum equaled one, thereby attributing equal importance to both classes despite their differing representation in the dataset.

2.3. Methods

2.3.1. Learnable Weights Graph Convolution Network (LWGCN)

Inspired by Ouyang et al. [18], the proposed model involves employing a GNN for ice and water classification. The first step is converting SAR imagery into graph-structured data. For an illustration, the original SAR image for an arbitrary chosen date (2017-01-12) is shown in Figure 2a for the Beauharnois Canal; we used a similar approach for Lake Saint Lawrence. To achieve the segmentation of the SAR image, we utilized the SLIC algorithm for segmenting the image into superpixels. The SLIC effectively groups pixels into coherent regions. A segmented graph is shown in Figure 2b. To construct a graph, we considered the centroids of these superpixels as nodes and defined the edges by connecting these centers, shown in Figure 2c. The land area was subsequently excluded, see Figure 2d, and this is the graph structure used in the LWGCN model.

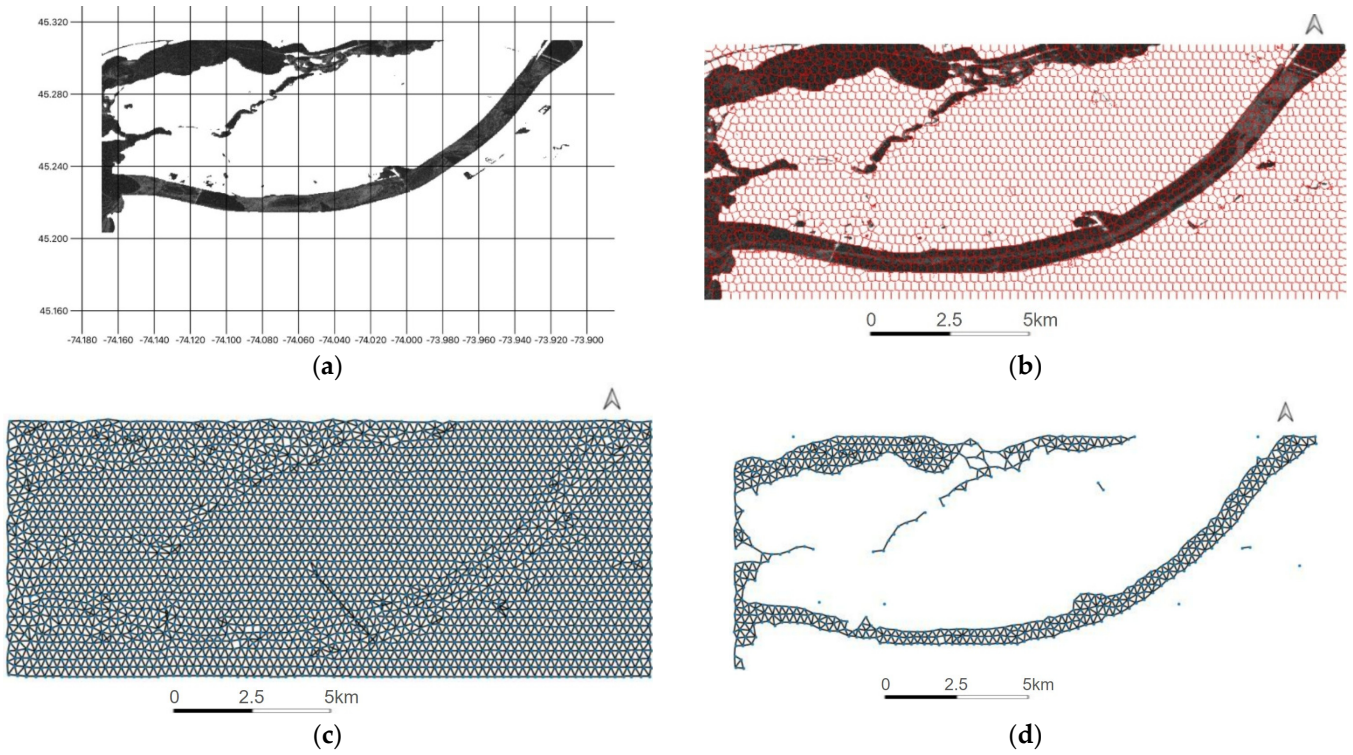

Figure 2. The process of generating graphs from SAR imagery for an arbitrary chosen date (2017-01-12) in the Beauharnois Canal. (**a**) Sentinel-1 SAR image. (**b**) Use simple linear iterative clustering (SLIC) to segment the image into superpixels. (**c**) Connect the centers of each superpixel. (**d**) Remove the land area (this is the graph structure used in the LWGCN model).

Our proposed approach to leveraging a GNN for the analysis of SAR imagery is anchored in the pioneering study by Kipf and Welling [10]. They proposed a GCN model structure consisting of a non-linear activation function, $\sigma(\cdot)$, usually using ReLu, propagation operator, $\boldsymbol{P}$, a feature matrix at the *lth* layer $\boldsymbol{H}^{(l)} \in R^{N\times Dl}$, and layer-specific learnable weights $\boldsymbol{W}^{(l)} \in R^{D_l\times D_{l+1}}$. At each layer, l, the features are updated by the features on the previous layer $l-1$. The equation governing the GCN operation is [10]

$$\mathbf{H}^{(1+1)} = \sigma\left(\mathbf{P}\mathbf{H}^{(1)}\mathbf{W}^{(1)}\right) \tag{1}$$

To prevent the values in the hidden states from exploding during the weighted multiplication, a normalization step can be applied to the adjacency matrix using the diagonal node degree matrix $\widetilde{D}$ of $\widetilde{A}$, ensuring each row sums to one. Kipf et al. [10] recommend node E denotes the number of edges, $\mathbf{P} = \widetilde{\boldsymbol{D}}^{-\frac{1}{2}}\widetilde{\boldsymbol{A}}\widetilde{\boldsymbol{D}}^{-\frac{1}{2}}$ with the degree matrix $\boldsymbol{D} \in \boldsymbol{R}^{N\times N}$ and adjacency matrix $\boldsymbol{A} \in R^{N\times N}$. Additionally, $\widetilde{\boldsymbol{A}} = \boldsymbol{A} + \boldsymbol{I}_N$ and $\widetilde{\boldsymbol{D}} = \boldsymbol{D} + \boldsymbol{I}_N$ represent the adjacency and degree matrix with self-loops on the original graph, where $\boldsymbol{I}_N \in R^{N\times N}$ is the identity matrix. Our model is built upon the existing GCN framework. To capture the relationships between nodes and determine the relative importance of each connection, we introduced learnable weights on the edges. The modified equation is as follows

$$\mathbf{H}^{(1+1)} = \sigma\left((\mathbf{P}\mathbf{E})\mathbf{H}^{(1)}\mathbf{W}^{(1)}\right) \tag{2}$$

Additional parameter $\mathbf{E} \in \mathrm{R}_n$ is applied to each edge in the normalized adjacency matrix $\mathbf{P}$. After experimenting with different initial weight settings, either as random values or set to $\mathbf{1}_{n\times n}$, we observed that initializing the weights to $\mathbf{1}_{n\times n}$ yields better performance. The node features we adapted in this model are listed in Table 1, where the intensity

is calculated by averaging the intensity at each superpixel. The standard deviation is calculated as follows:

$$\text{standard deviation} = \sqrt{\frac{1}{N}\sum_{i=1}^{N}(x_i - \mu)^2} \quad (3)$$

where N is the number of pixels, μ is the mean of the intensities, and x_i is the pixels inside each superpixel. The standard deviation is calculated for each superpixel, recording the variance of intensity on the map. In the ice and water classification task, ice and water exhibit distinct variance patterns due to their reflectance in the SAR data. Ice, with its textured appearance, results in a higher standard deviation, while water generally shows lower variance. We only used variance as the SAR texture features because, similar to [19], we did not find higher order features, such as those from grey-level co-occurence matrices, to be useful for our problem. The air temperature is mapped to each superpixel in the domain. The model architecture is listed in Table 2. Our model begins with an LWGCN layer with an input size defined by the number of nodes and features, as shown in the equation.

Table 1. Geometric, texture, and environmental features computed for each node in the LWGCN model.

Number	Features	Category
1	Intensity	Textural
2	Standard deviation	Textural
3	Air temperature	Environmental

Table 2. The LWGCN model architecture, where n is the number of nodes, h is the hidden size, and *cout* is the output size.

Input Size	Layer	Output Size
$n \times$ Number of features	LWGCN layer	$n \times h$
$n \times h$	ReLU	$n \times h$
$n \times h$	Dropout layer	$n \times h$
$n \times h$	LWGCN layer	$n \times c_{out}$
$n \times c_{out}$	Log Softmax	$n \times c_{out}$

This is followed by a ReLU activation function and then a dropout layer. Another LWGCN layer follows the dropout layer. Finally, a log softmax function is applied to produce the output.

2.3.2. Support Vector Machine (SVM)

SVMs [20] classify ice and water in SAR images by learning from the same feature vectors as the GNN. During training, SVMs find an optimal hyperplane to separate data points into ice and water, maximizing the margin between the closest points of each class. We optimized the regularization strength parameter, C, to 10, balancing training and testing error, and set the gamma parameter to 1 to observe its effect. The radial basis function (RBF) kernel was selected after testing.

2.3.3. Convolutional Neural Network (CNN)

The CNN has three convolutional layers with filter sizes of 32, 64, and 128 and kernel sizes of 7×7, 5×5, and 3×3, followed by three groups of residual blocks. Max pooling layers downsample, and dropout layers with a 0.5 rate prevent overfitting. An adaptive average pooling layer reduces spatial dimensions to 1×1, which is flattened and

passed through two fully connected layers, ending with a sigmoid activation for binary classification. ReLU activation is applied after each convolution within the residual blocks.

2.4. Experimental Set-Up

We adopted the Adam optimizer [21], and we conducted an exhaustive grid search to fine-tune the hyperparameters, ensuring optimal model convergence and effectiveness. The specific hyperparameter configurations utilized are documented in Table 3. To facilitate our research on GNNs, we utilized the PyTorch [22] and PyTorch-Geometric [23] libraries. Our computational experiments were executed on the Cedar cluster by Compute Canada on A100 GPU. The entire dataset comprised SAR imagery from the winter months (January to March) for the years 2017 to 2021, capturing the temporal evolution of environmental conditions. Cross-validation was used to assess model performance by dividing the dataset into five subsets, each representing one year from 2017 to 2021. In each iteration, one year is held out as the test set, while the remaining four years are used for training. This process is repeated five times, ensuring each year is tested once. The performance metrics from each iteration are aggregated to provide an overall assessment, ensuring a robust evaluation of the model's ability to predict across different years. The convergence of our model is set to 20 epochs. The choice of 20 epochs was determined based on preliminary experiments that indicated this number of epochs was generally sufficient for observing convergence behavior in our specific task without overfitting.

Table 3. Hyper-parameters used in the LWGCN model over the Lake Saint Lawrence for years 2017 to 2021.

Loss	Learning Rate	Weight Decay	Channels	Dropout	Hidden Size (h)
Cross Entropy Loss	0.01	5×10^{-4}	2	0.2	4

3. Results

We present a comparative analysis of our proposed GNN approach for classifying ice and water in SAR images with GCN, CNN, and SVM models on both the Beauharnois Canal and Lake Saint Lawrence. The evaluation criteria include classification accuracy and computational efficiency. Our LWGCN method demonstrates superior classification accuracy compared to other models. Due to the simplicity of the ice condition of the Beauharnois Canal, there is minimal difference in performance among the methods. Therefore, we focused more on the results for Lake Saint Lawrence. Table 4 presents the model accuracy from 2017 to 2021 for the four different methods tested on Lake Saint Lawrence.

Table 4. Binary average accuracies of different models for different years in percentage. The best performances are highlighted in bold.

Model	2017	2018	2019	2020	2021
GCN	84.3723	79.1782	83.2189	75.8912	82.6316
SVM	62.1278	78.2825	72.1287	65.1813	81.9825
CNN	80.1228	77.9495	83.2096	77.3942	86.2384
LWGCN	**84.6034**	**81.3472**	**85.4234**	**88.0293**	**88.6345**

The accuracy is calculated by comparing the predicted labels to the true labels. For binary classification tasks, the model's output is first passed through a sigmoid function, and the results are rounded to obtain binary predictions. The number of correct predictions is then summed and divided by the total number of samples to yield accuracy. Our LWGCN model outperforms the other three approaches. The LWGCN model excels in capturing these complexities by effectively learning features from the spatial surroundings through its adaptive weighting of the edges in the graph. We also selected a specific date, 2018-01-07, as a reference date. We chose this date because there is a very prominent shipping lane across the lake, which appears brighter than its surroundings. This brightness is due to the ship

breaking the ice, leaving a trail of broken ice with high backscatter. The LWGCN model output for an arbitrary date, 2018-01-07, is shown in Figure 3, and the color indications are shown in Table 5. Based on this figure, it is evident that there were minimal errors in classifying the shipping lane, with surrounding areas correctly identified as ice. This accuracy is attributed to the capability of GNNs to capture spatial relationships effectively.

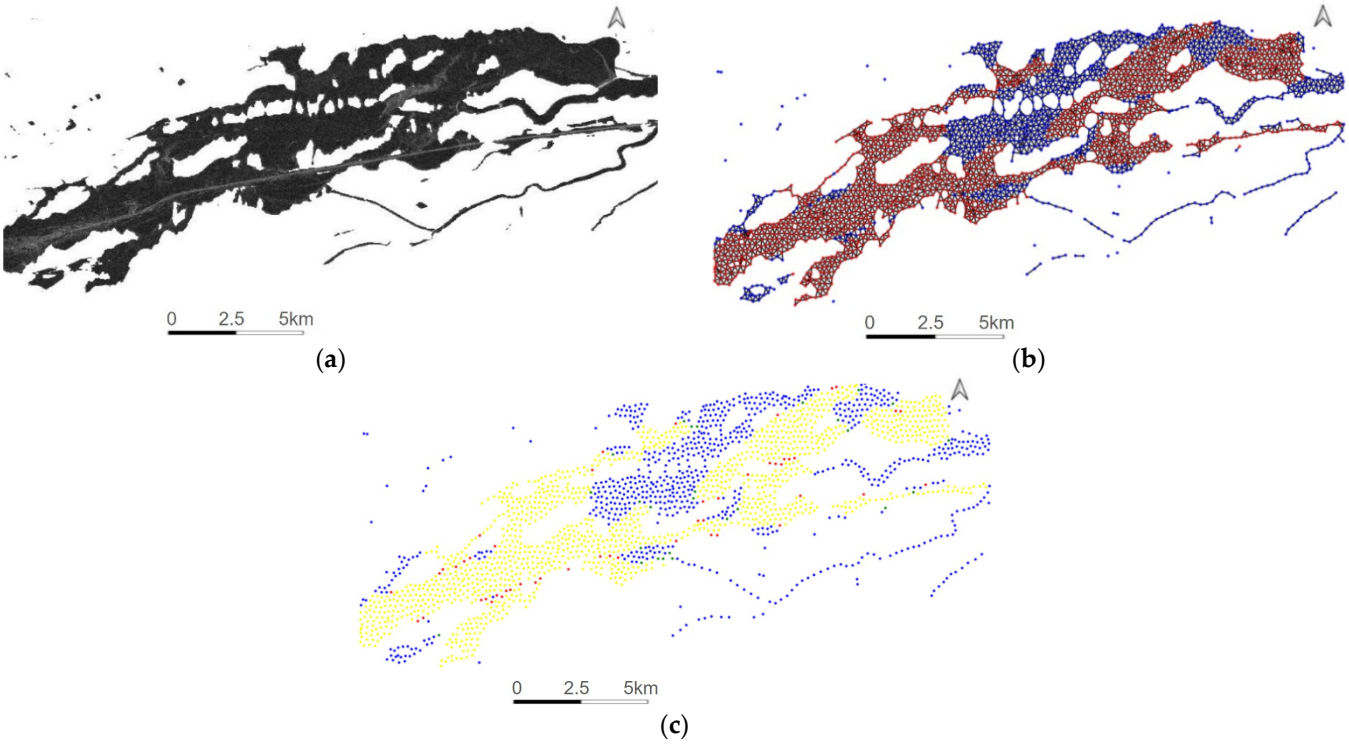

Figure 3. (**a**) Sentinel-1 VV SAR image of Lake Saint Lawrence (see Figure 1 for location within larger study region), (**b**) ground truth from manually labeled shapefile, where blue indicates water and red indicates ice, and (**c**) LWGCN model output, where the colors are represented in Table 5. The arbitrary chosen date is 2018-01-07.

Table 5. The color presentation in the LWGCN model output image.

	Correctly Labeled	**Incorrectly Labeled**
Ice	Yellow	Green
Water	Blue	Red

Our method of using graphs to classify ice and water reduces the time it needs to train and predict the result. Table 6 records the time it needs to train 20 epochs on Lake Saint Lawrence; our LWGCN is about 8 times faster than the CNN method.

Table 6. Processing time in seconds for different models for different years. The best times are highlighted in bold.

Time (s)	**2017**	**2018**	**2019**	**2020**	**2021**
CNN	3992.1835	3827.0839	3893.7901	3993.2819	3940.2834
LWGCN	**554.3452**	**453.4839**	**593.2892**	**468.3008**	**532.9503**

4. Discussion

In this study, we evaluated the performance of LWGCN, GCN, CNN, and SVM models for classifying ice and water in SAR images, focusing on Lake Saint Lawrence. Our results,

as depicted in Table 4, underscore the superior performance of LWGCN compared to GCN, CNN, and SVM across the years 2017–2021. This superiority is particularly pronounced given the complex ice conditions of Lake Saint Lawrence, where LWGCN consistently achieved higher accuracy. Notably, the model's ability to leverage spatial relationships effectively enabled accurate classification of intricate features such as shipping lanes and ice formations (Figure 3). Comparing our findings with traditional CNN and SVM approaches, we observed that LWGCN outperformed in scenarios requiring nuanced spatial understanding. Between the two GNNs, we observe that our proposed model LWGCN slightly outperforms GCN. This improvement can be attributed to the additional learnable weights assigned to the edges in LWGCN. Despite the promising outcomes, our study encountered limitations related to dataset availability and feature variability. Future research will prioritize expanding datasets to encompass diverse environmental conditions and enhancing the variability of node features. This can be achieved by incorporating additional parameters such as shape index, bathymetry, and river width [24]. Additionally, exploring advanced GNN architectures, integrating multi-modal data sources, and conducting field validation studies could further enhance the model robustness and applicability in real-world settings.

5. Conclusions

After evaluating the performance of different models including LWGCN, GCN, CNN, and SVM, for classifying ice–water in SAR imagery, the findings indicate that leveraging graph-based neural networks, especially LWGCN, can significantly enhance the accuracy of ice and water classification in SAR imagery. Despite the promising results, the study highlights the need for future research to expand the diversity of datasets and incorporate additional environmental features such as river corridor slope, effective width, and river shape index [24]. These enhancements could further improve the models' robustness and applicability in varying conditions. This study underscores the potential of LWGCN in remote sensing applications, paving the way for more advanced and precise environmental monitoring.

Author Contributions: Conceptualization, methodology, validation: K.A.S., D.S., Y.Q. and A.S.; Software: Y.Q. and A.S.; Writing-original draft preparation: Y.Q., A.S. and K.A.S.; Writing - review and editing: Y.Q., A.S. and K.A.S.; Project administration: D.S. and K.A.S. All authors have read and agreed to the published version of the manuscript.

Funding: This research was funded by Global Water Futures (GWF) and the National Research Council of Canada (NRC). NRC provided funding through its Climate Resilient Built Environment Initiative, in support of delivering the Government of Canada's Adaptation Action Plan, and towards achieving commitments under the National Adaptation Strategy. The initial work was also supported by the International Joint Commission (IJC), as part of a project carried out by the NRC.

Institutional Review Board Statement: Not applicable.

Informed Consent Statement: Not applicable.

Data Availability Statement: The original data presented in the study are openly available in https://github.com/Maruko1337/RiverIceProject (accessed on 25 November 2024).

Acknowledgments: We would like to acknowledge funding from Global Water Futures as well as the National Research Council of Canada. Computing resources were provided by the Digital Research Alliance of Canada.

Conflicts of Interest: The authors declare no conflicts of interest.

References

1. Guo, X.; Wang, T.; Fu, H.; Guo, Y.; Li, J. Ice-jam forecasting during river breakup based on neural network theory. *J. Cold Reg. Eng.* **2018**, *32*, 04018010. [CrossRef]
2. Dierking, W. Sea ice monitoring by synthetic aperture radar. *Oceanography* **2013**, *26*, 100–111. [CrossRef]
3. Singh, A.; Kalke, H.; Loewen, M.; Ray, N. River ice segmentation with deep learning. *IEEE Trans. Geosci. Remote Sens.* **2020**, *58*, 7570–7579. [CrossRef]

4. Zhang, X.; Jin, J.; Lan, Z.; Li, C.; Fan, M.; Wang, Y.; Yu, X.; Zhang, Y. ICENET: A semantic segmentation deep network for river ice by fusing positional and channel-wise attentive features. *Remote Sens.* **2020**, *12*, 221. [CrossRef]
5. Ansari, S.; Rennie, C.; Clark, S.; Seidou, O. IceMaskNet: River ice detection and characterization using deep learning algorithms applied to aerial photography. *Cold Reg. Sci. Technol.* **2021**, *189*, 103324. [CrossRef]
6. Sola, D.; Scott, K.A. Efficient Shallow Network for River Ice Segmentation. *Remote Sens.* **2022**, *14*, 2378. [CrossRef]
7. Xu, L.; Clausi, D.A.; Li, F.; Wong, A. Weakly supervised classification of remotely sensed imagery using label constraint and edge penalty. *IEEE Trans. Geosci. Remote Sens.* **2016**, *55*, 1424–1436. [CrossRef]
8. Shao, Y.; Sang, N.; Gao, C.; Ma, L. Spatial and class structure regularized sparse representation graph for semi-supervised hyperspectral image classification. *Pattern Recognit.* **2018**, *81*, 81–94. [CrossRef]
9. Zhao, Y.; Su, F.; Yan, F. Novel semi-supervised hyperspectral image classification based on a superpixel graph and discrete potential method. *Remote Sens.* **2020**, *12*, 1528. [CrossRef]
10. Kipf, T.N.; Welling, M. Semi-supervised classification with graph convolutional networks. In Proceedings of the International Conference on Learning Representations, San Juan, Puerto Rico, 2–4 May 2016.
11. Achanta, R.; Shaji, A.; Smith, K.; Lucchi, A.; Fua, P.; Süsstrunk, S. SLIC Superpixels. 2010. Available online: https://www.researchgate.net/publication/44234783_SLIC_superpixels (accessed on 1 June 2024).
12. Sudom, D.; Barrette, P.; Burcher, R. Plausible Scenarios for Future Ice Conditions in the St. Lawrence River. In Proceedings of the Prepared for: International Joint Commission (IJC) Great Lakes-St. Lawrence River Adaptive Management (GLAM) Committee, Cornwall, ON, Canada, 4–5 October 2024.
13. Alaska Satellite Facility. Alaska Satellite Facility Search. Available online: https://search.asf.alaska.edu (accessed on 1 June 2024).
14. NASA. Worldview: Explore Your Dynamic Planet. Available online: https://worldview.earthdata.nasa.gov (accessed on 1 June 2024).
15. Esri. Sentinel-2 Land Cover Explorer. Available online: https://livingatlas.arcgis.com/landcoverexplorer (accessed on 1 June 2024).
16. Government of Canada. Climate Data: Moose Creek Wells. Available online: https://climate.weather.gc.ca (accessed on 1 June 2024).
17. Korosov, A.; Demchev, D.; Miranda, N.; Franceschi, N.; Park, J.W. Thermal denoising of cross-polarized Sentinel-1 data in interferometric and extra wide swath modes. *IEEE Trans. Geosci. Remote Sens.* **2021**, *60*, 1–11. [CrossRef]
18. Ouyang, S.; Li, Y. Combining deep semantic segmentation network and graph convolutional neural network for semantic segmentation of remote sensing imagery. *Remote Sens.* **2020**, *13*, 119. [CrossRef]
19. Chu, T.; Das, A.; Lindenschmidt, K.E. Monitoring the Variation in Ice-Cover Characteristics of the Slave River, Canada Using RADARSAT-2 Data—A Case Study. *Remote Sens.* **2015**, *7*, 13664–13691. [CrossRef]
20. Cortes, C.; Vapnik, V. Support-vector networks. *Mach. Learn.* **1995**, *20*, 273–297. [CrossRef]
21. Kinga, D.; Adam, J.B. A method for stochastic optimization. In Proceedings of the International Conference on Learning Representations (ICLR), San Diego, CA, USA, 7–9 May 2015.
22. Paszke, A.; Gross, S.; Massa, F.; Lerer, A.; Bradbury, J.; Chanan, G.; Killeen, T.; Lin, Z.; Gimelshein, N.; Antiga, L.; et al. Pytorch: An imperative style, high-performance deep learning library. *Adv. Neural Inf. Process. Syst.* **2019**, *32*, 8026–8037.
23. Fey, M.; Lenssen, J.E. Fast graph representation learning with PyTorch Geometric. In Proceedings of the ICLR Workshop on Representation Learning on Graphs and Manifolds, New Orleans, LA, USA, 6–9 May 2019.
24. Chu, T.; Lindenschmidt, K.E. Effects of river geomorphology on river ice freeze-up and break-up rates using MODIS imagery. *Can. J. Remote Sens.* **2019**, *45*, 176–191. [CrossRef]

Disclaimer/Publisher's Note: The statements, opinions and data contained in all publications are solely those of the individual author(s) and contributor(s) and not of MDPI and/or the editor(s). MDPI and/or the editor(s) disclaim responsibility for any injury to people or property resulting from any ideas, methods, instructions or products referred to in the content.